Journal of Catalysis 266 (2009) 343–350

Contents lists available at ScienceDirect

Journal of Catalysis

journal homepage: www.elsevier.com/locate/jcat

Oxide-supported single gold catalyst for selective hydrogenation of acrolein predicted from first principles

Chuan-Ming Wang, Kang-Nian Fan, Zhi-Pan Liu *

Shanghai Key Laboratory of Molecular Catalysis and Innovative Materials, Department of Chemistry, MOE Key Laboratory for Computational Physical Sciences, Fudan University, Shanghai 200433, China

ARTICLE INFO

Article history:
Received 4 February 2009
Revised 24 June 2009
Accepted 28 June 2009
Available online 28 July 2009

Keywords:
Single-site heterogeneous catalysis
Density functional theory calculations
Selective hydrogenation of acrolein
Gold catalysis

ABSTRACT

The searching for more practical applications of single-site heterogeneous catalysis has attracted much attention recently. Here the hydrogenation of acrolein on AuOH/m-ZrO_2 is extensively investigated theoretically aiming to verify whether a desired selectivity toward allyl alcohol can be achieved. Although similar hydrogenation reactions have been reported for Au/oxides catalysts in experiment, it is not clear what the active Au component is. In this work we evaluate both the stability and the activity of single Au supported on monoclinic ZrO_2 surfaces from first principles. Our calculated results indicate that Au clusters are the most stable form on the flat m-ZrO_2 surface, while single Au cations can be available on the stepped m-ZrO_2 sites below 350 K at ambient (oxidizing) conditions. Importantly, we demonstrate that the minority species, AuOH/m-$ZrO_2(\bar{2}12)$, exhibits the desired catalytic selectivity for the hydrogenation of acrolein. The deep hydrogenation to propyl alcohol can also be prevented kinetically on this single-site heterogeneous catalyst.

1. Introduction

The selective hydrogenation of α,β-unsaturated aldehydes ($R_1R_2C{=}CH{-}CH{=}O$) to unsaturated alcohols ($R_1R_2C{=}CH{-}CH_2OH$) is a challenging topic in chemistry. For the wide application of unsaturated alcohols in fine chemical industry, it is highly desirable to perform this reaction in heterogeneous conditions with a high selectivity. However, it was found that the major products are saturated aldehydes or saturated alcohols when using conventional hydrogenation catalysts. This is understandable as the hydrogenation of the C=C bond of $R_1R_2C{=}CH{-}CH{=}O$ is thermodynamically more favorable over the hydrogenation of the C=O bond [1]. In this work, we propose a new model catalyst, namely, single Au supported on m-ZrO_2, for the hydrogenation of acrolein. We predict by theory that a desired selectivity can be achieved on this single-site heterogeneous catalyst.

On the traditional hydrogenation catalyst, platinum (Pt) metal, the selectivity for the hydrogenation of α,β-unsaturated aldehydes was found to be sensitive to many factors, for example, the structure and morphology of metal particles, the support materials, and the reaction conditions [1–3]. Theoretically, density functional theory (DFT) calculations have been utilized to understand the reaction mechanism [4–9]. The calculations by Sautet group showed that the substitute group (R_1 and R_2) and the surface coverage can significantly affect the adsorption structure of α,β-unsaturated aldehydes on Pt surface [9,10]. A major problem of Pt catalyst is that the desorption of partial hydrogenation products competes with the hydrogenation steps, which leads to a poor selectivity [5]. Recently, some progress has been made by alloying Pt catalysts with other promoters (Fe, Sn) or choosing other less active metals such as Ag and Au [11–15].

In particular, experimental results showed that the newly emerged supported gold catalysts can exhibit very high selectivity for the hydrogenation of α,β-unsaturated aldehydes [16–21]. Bailie et al. found that Au/ZrO_2 and Au/ZnO can catalyze the hydrogenation of crotonaldehyde to crotyl alcohol with the selectivity being 81%, showing that the hydrogenation of the C=O bond is favored over that of the C=C bond [19,21]. The selective hydrogenation of acrolein was then tested over a variety of supported gold catalysts, including Au/SiO_2, Au/ZrO_2, Au/TiO_2, Au/ZnO, and Au–In/ZnO [11,20,22–26]. The nature of the active Au species in these catalysts remains controversial.

In addition to nano-gold particles being considered as active components, recent studies also suggested that the smallest Au unit, single Au cation, might be enough for catalyzing hydrogenation reactions [27–32]. This is exciting as the cost of noble metal catalysts can be reduced dramatically. Guzman and Gates deposited mononuclear Au complexes on MgO oxide and found that such a catalyst can catalyze ethene hydrogenation. They speculated that Au^{III} complexes are the catalytically active species

* Corresponding author. Fax: +86 21 6564 2400.
E-mail address: zpliu@fudan.edu.cn (Z.-P. Liu).

0021-9517/$ - see front matter © 2009 Elsevier Inc. All rights reserved.
doi:10.1016/j.jcat.2009.06.023

[29]. Zhang et al. also reported that single Au species supported on ZrO_2 are the active site for the hydrogenation of 1,3-butadiene [31]. Using DFT calculations, we demonstrated that Au^I is the active Au species that catalyzes the hydrogenation of 1,3-butadiene to butene [33].

Motivated by the previous findings on single Au catalyzed hydrogenation, here we further explore the activity and selectivity of single Au catalysts aiming to design better materials for the hydrogenation of α,β-unsaturated aldehydes. Au/m-ZrO_2 is chosen as the model catalyst for the hydrogenation of acrolein considering that m-ZrO_2 is the most popular phase of ZrO_2 in typical catalyst preparation conditions. This paper is organized as follows. The calculation details and the modeling will be briefly summarized in Section 2. The structures and stabilities of single Au species on m-ZrO_2, and the hydrogenation mechanism of acrolein are addressed in Section 3. The conclusions are drawn in Section 4.

2. Computational methods and modeling

All DFT periodic calculations were performed using SIESTA package with numerical atomic orbital basis sets and Troullier–Martins norm-conserving pseudopotentials (scalar relativistic for heavy elements) [34–36]. The semicore states (4s, 4p) for Zr had been treated explicitly. The exchange-correlation functional utilized in this work was at the level of the generalized gradient approximation (GGA), known as GGA-PBE [37]. The double-ζ plus polarization (DZP) numerical atomic orbitals were employed as the basis sets for all elements. The orbital-confining cutoff radii were determined from an energy shift of 0.01 eV. The energy cutoff for the real space grid used to represent the density was set as 150 Ry. The Broyden method was employed for geometry relaxation until the maximal forces on each relaxed atom were less than 0.1 eV/Å. The recently developed constrained Broyden minimization method was employed to search for the transition state (TS) of reaction [38–41]. For some key reactions, TSs have been validated by numerical Hessian analysis, which confirm that the calculated TSs have one and only one imaginary mode. These DFT calculation setups were also utilized in our previous works [38–41], where the convergence on the calculated barrier has been carefully benchmarked with the calculations using the plane-wave methods.

To know the exact structure of Au monomers on ZrO_2 is the first step for a systematic understanding of the selective hydrogenation of acrolein. We considered three possible different Au monomers on ZrO_2, namely, Au atom (Au^0), AuOH (Au^I), and $Au(OH)_3$(Au^{III}). Monoclinic ZrO_2 (m-ZrO_2) was chosen as the support since it is the most stable phase of ZrO_2. Both flat and stepped-ZrO_2 surfaces were then employed to anchor three Au monomers. Theoretically, the surface structure and stability of ZrO_2 (as measured by surface energy) were thoroughly investigated by Christensen et al. using the plane-wave DFT method [42]. The detailed surface structure has also been addressed in our previous work [43,44]. The most stable m-$ZrO_2(\bar{1}11)$ surface is modeled to represent the flat surface. The stepped m-$ZrO_2(\bar{2}12)$ is modeled to represent the stepped surface, which contains both m-$ZrO_2(\bar{1}11)$ terraces and m-$ZrO_2(\bar{1}01)$ steps. As the stepped m-$ZrO_2(\bar{1}01)$ is the facet of the second-lowest surface energy, this type of steps should be the most common structural defects in m-ZrO_2. Because of the large unit cell used m-$ZrO_2(\bar{1}11)$ [$p(2\times2)$, 13.63 Å × 14.75 Å], m-$ZrO_2(\bar{2}12)$ [$p(2\times1)$, 13.63 Å × 11.69 Å]}, only Γ-point was used to sample the first Brillouin zone. The convergence of barriers with respect to k-point sampling up to a $(2\times2\times1)$ mesh has been checked and the error bar is found to be within 0.05 eV for the calculated barrier.

3. Results and discussion

3.1. Structure of Au monomers on m-ZrO_2 surface

To investigate the structure of Au monomers, we deposited three most-likely forms of Au monomers, namely, Au^0, Au^I, and Au^{III} on both the flat and the stepped m-ZrO_2 surfaces. The structures of each form were optimized from the initial configurations provided by Nose thermostat molecular dynamics at 300 K for a few picoseconds. The thermodynamic stability of the Au monomers was measured by the reaction energies ΔE_f according to the following formula:

$$Au(OH)_3 + ZrO_2 \rightarrow Au/ZrO_2 + 3/2H_2O + 3/4O_2 \quad (1)$$

$$Au(OH)_3 + ZrO_2 \rightarrow AuOH/ZrO_2 + H_2O + 1/2O_2 \quad (2)$$

$$Au(OH)_3 + ZrO_2 \rightarrow Au(OH)_3/ZrO_2 \quad (3)$$

These formula describe the formation of m-ZrO_2 supported Au monomers from the $Au(OH)_3$ (Au^{III}) precursor as a mimic of the typical experimental procedure, where Au is deposited onto oxides in $HAuCl_4$ solution at ambient (oxidizing) condition. Here ΔE_f is defined as the DFT total energy (E) difference between the reactants and the products (E, strictly speaking, the Helmohotz free energy at 0 K and neglecting zero-point vibrations). Our calculated values of ΔE_f are listed out in Table 1, and their corresponding structures are shown in Fig. 1. To deduce the free energies at finite temperature and pressure, we performed the following thermodynamic calculations. For solid state reactions, the DFT total energy is a good approximation to the Gibbs free energy (G) as the temperature and pressure (T, p) contribution is small. For molecules in the gas phase such as O_2 and H_2O, E is quite different from G at elevated temperatures due to the large entropy contribution. We utilized the standard thermodynamic data to estimate the temperature contribution to the free energy of the gas phase H_2O and O_2 at finite temperatures according to Eqs. (4) and (5) [45]

$$\mu_X(T,P_X) = \tilde{\mu}_X\left(T,P^0\right) + k_B T \ln\left(\frac{P_X}{p^0}\right) \quad (4)$$

$$\tilde{\mu}_X\left(T,P^0\right) = \left[H_X\left(T,P^0\right) - H_X\left(0\,K,P^0\right)\right] - T\left[S_X\left(T,P^0\right) - S_X\left(0\,K,P^0\right)\right] \quad (5)$$

We compared ΔG_f of the Au monomers in Fig. 2, where ΔG_f is plotted against temperature. ΔG_f of metallic Au cluster can also be deduced from ΔG_f of Au^0 according to the calculated cohesive energy of Au clusters (~3.0 eV) [46].

From the calculated most stable structures shown in Fig. 1, we can see that the most stable form of AuOH on m-ZrO_2 has a two-coordinated linear structure, and that of $Au(OH)_3$ has a four-coordinated quasi-planar structure. In both cases at least one lattice O (O_{latt}) takes part in the bonding with the cationic Au and the Au–O bond distance is about 2.10 Å. Furthermore, the OH groups attached to the Au cation have to be stabilized by the surface Zr cations. This leads to the formation of Au–O–Zr linkages. Such

Table 1
Reaction energy (ΔE_f) of Au monomers on m-$ZrO_2(\bar{1}11)$ and m-$ZrO_2(\bar{2}12)$ surfaces at oxidizing (Eqs. (1)–(3)) and reducing (Eqs. (6) and (7)) conditions. The energy unit is eV.

	Au^0 atom	AuOH	$Au(OH)_3$
Oxidizing condition (Eqs. (1)–(3))			
m-$ZrO_2(\bar{1}11)$	0.40	−1.87	−2.11
m-$ZrO_2(\bar{2}12)$	0.29	−2.33	−4.09
Reducing condition (Eqs. (6) and (7))			
m-$ZrO_2(\bar{1}11)$	−3.30	−4.33	−2.11
m-$ZrO_2(\bar{2}12)$	−3.41	−4.79	−4.09

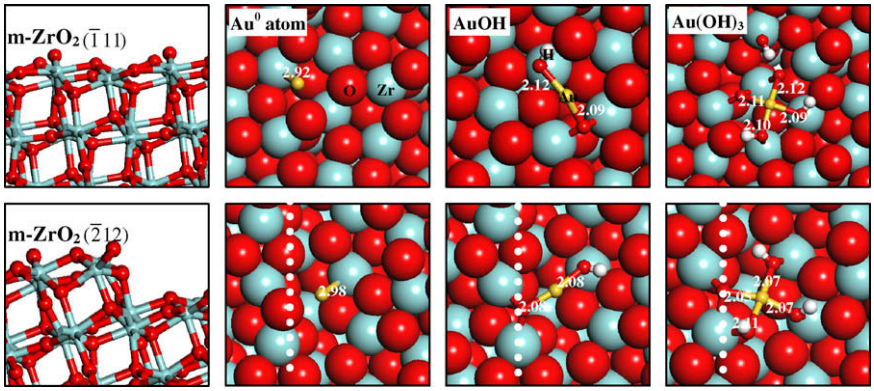

Fig. 1. Side views of m-$ZrO_2(\bar{1}11)$ and m-$ZrO_2(\bar{2}12)$ surfaces and top views of three different Au monomers on the m-ZrO_2 surfaces. The distance of important bonds (Au–O or Au–Zr bond) are also listed (the unit is Å). The dotted lines are drawn along the step-edges for the guide of eye.

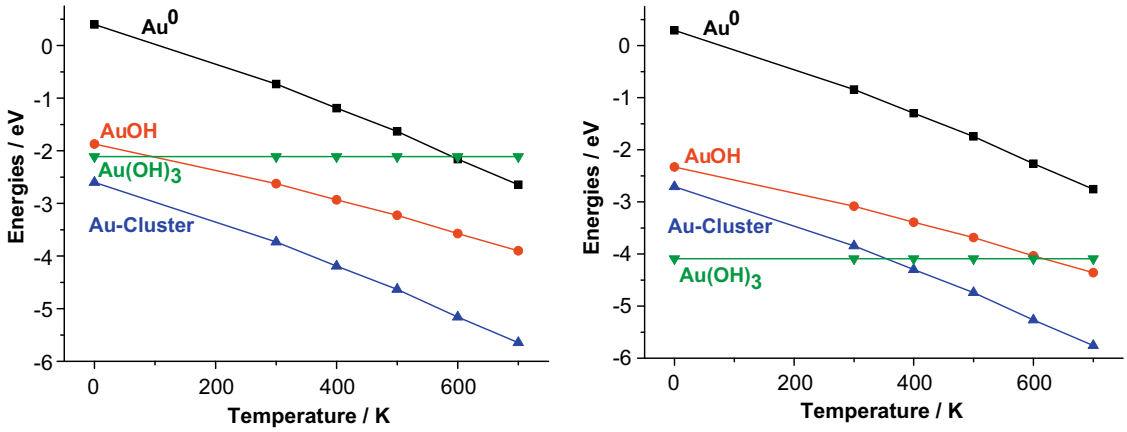

Fig. 2. Temperature dependence of the reaction-free energies of Au monomers (Au^0, Au^I, Au^{III}) and metallic Au cluster on the flat m-$ZrO_2(\bar{1}11)$ (left) and the stepped m-$ZrO_2(\bar{2}12)$ (right) surfaces.

supported cationic Au complexes mimic their counterparts in solution as found in homogeneous catalysis [47,48]. It is clear that a suitable local geometry of lattice O and Zr atoms is required in order to achieve the particular coordination geometry for cationic Au. In this sense, surface defected sites are more advantageous, where more anchoring sites are available. By contrast, a significant surface structure relaxation is necessary for the oxide terrace to bond with Au monomers. For example, we found that a Zr–O_{latt} bond has to break in order to achieve the quasi-planar structure for $Au(OH)_3$ on m-$ZrO_2(\bar{1}11)$ (see Fig. 1). This additional energy cost may explain why the Au cations on the flat m-$ZrO_2(\bar{1}11)$ surface are less stable.

From Table 1 and Fig. 2, it is clear that the stepped m-ZrO_2 sites are generally preferred by Au monomers compared to the flat m-ZrO_2 sites. This is consistent with the previous results for Au monomers on t-ZrO_2 surface [33]. $Au(OH)_3$ (Au^{III}) at the stepped m-ZrO_2 is thermodynamically the most stable Au monomer at 0 K with ΔE_f being −4.09 eV, and it remains to be stable at the oxide defect up to 350 K (see Fig. 2). With the increase of temperature, $Au(OH)_3$ is finally reduced toward the formation of Au clusters from the thermodynamic point of view. By contrast, on the terrace of the oxide only metallic Au clusters are stable thermodynamically. Considering the dominance of the terrace sites, it is therefore not surprising to observe Au clusters on oxides in experiment. The neutral Au atom (Au^0) is the least stable one and adsorbs only weakly on m-ZrO_2 surfaces. It can thus be concluded that both the temperature and the oxide structure are critical to the exact form and the oxidation state of Au in the calcination procedure of Au/oxides catalysts. Single Au catalyst (Au^{III} cation) may be present only at oxide defects and at relatively low temperatures.

3.2. Selective hydrogenation of acrolein

As $Au(OH)_3$ can be thermodynamically more stable than Au clusters at oxide steps at low temperatures. This provides the pos-

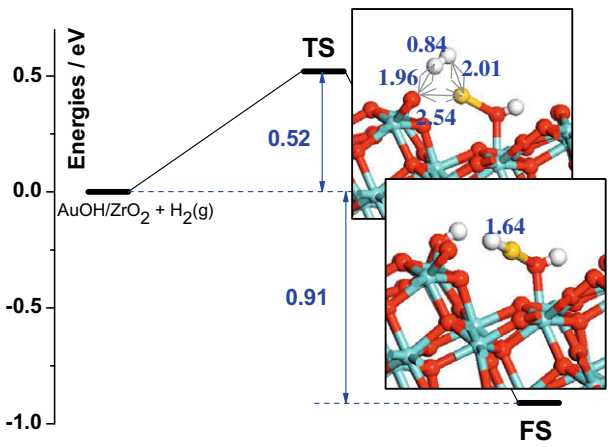

Fig. 3. Energy profile of H_2 dissociation on AuOH/m-$ZrO_2(\bar{2}12)$. Also shown are the structures (lateral views) of the TS and the final state (FS).

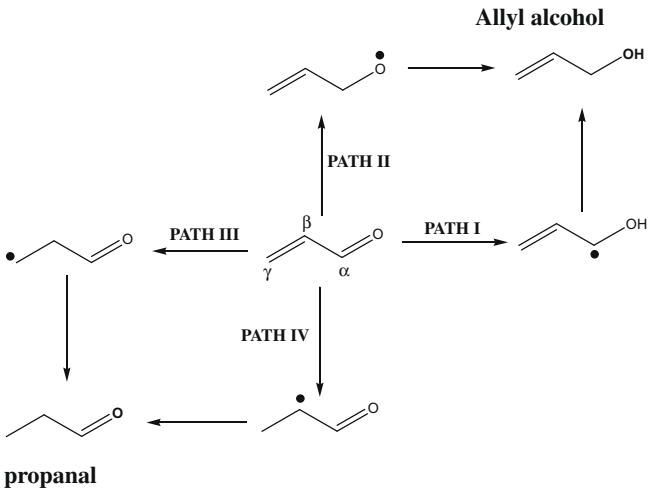

Scheme 1. Possible reaction routes for the hydrogenation of acrolein.

sibility to prepare in the first place the finely dispersed Au^{III} monomers at oxide defects after the calcination procedure, which should be carried out at mild oxidizing conditions. It is then interesting to examine whether these Au^{III} monomer can be a good single-site catalyst in the hydrogenation reactions, which, however, may reduced further to Au^{I} and Au^{0} in situ. The thermodynamic stability of Au^{0} and Au^{I} monomers under H_2 pressure conditions can be calculated similarly to those in Eqs. (1)–(3) according to the following formula:

$$Au(OH)_3 + ZrO_2 + 3/2H_2 \rightarrow Au/ZrO_2 + 3H_2O \quad (6)$$

$$Au(OH)_3 + ZrO_2 + H_2 \rightarrow AuOH/ZrO_2 + 2H_2O \quad (7)$$

The results are also listed out in Table 1, which showed that AuOH is thermodynamically the most stable monomer at the reducing environment. The reduction of $Au(OH)_3$ at the stepped sites of oxides to AuOH is therefore both thermodynamically and kinetically favored [33]. It should be mentioned that the sintering from $Au(OH)_3$ to bulky Au particles is prohibited kinetically at reaction conditions. This is because Au^{III} has already been highly dispersed and anchored at oxide defects, where the stepwise in situ conversion from Au^{III} to Au^{0} neutral atom needs to overcome high barrier. Obviously, the sintering into Au particles needs the presence of Au^{0} neutral atoms, which can migrate on the surface of oxides. Because Au^{0} is much more unstable compared to Au^{I} (Table 1), this process is kinetically difficult (a barrier is at least 1.3 eV from Au^{I} to Au^{0}) de-

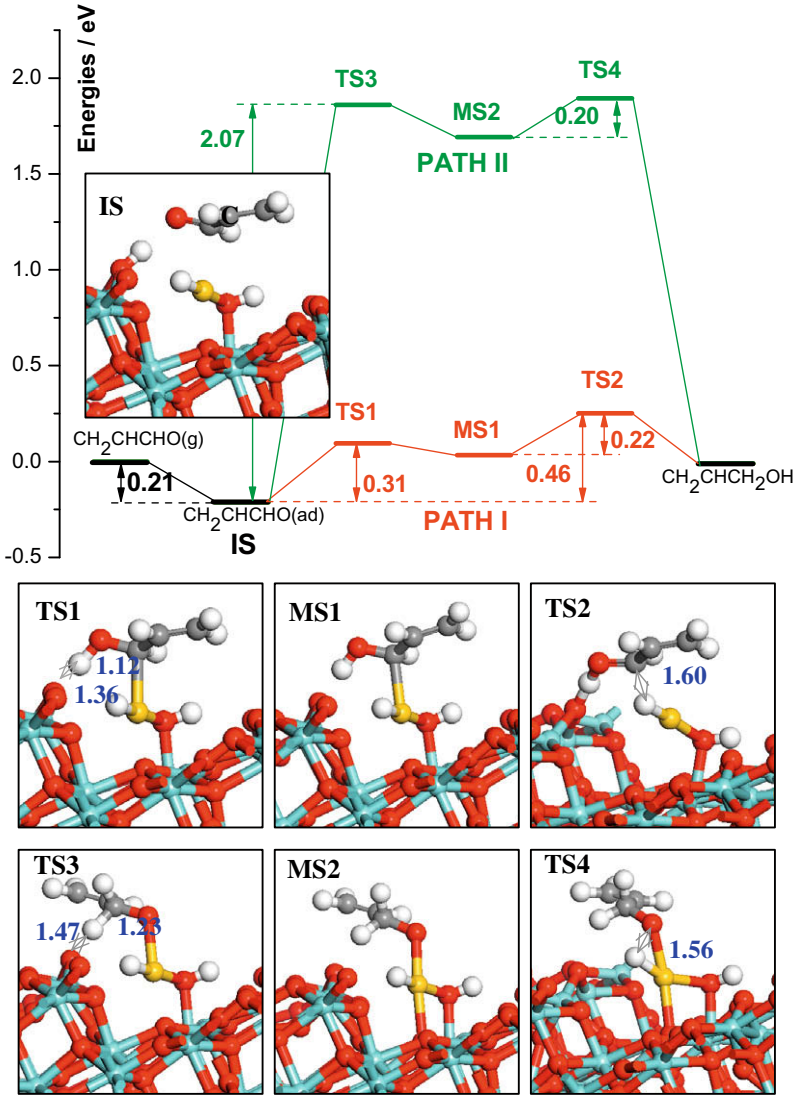

Fig. 4. Reaction profiles of the hydrogenation of acrolein to allyl alcohol on AuOH/m-$ZrO_2(\bar{2}12)$. Also shown are the structures (lateral views) of the IS, TS, and the MS.

spite the overall exothermicity in forming large Au particles at the reducing condition. Given these information, we directly chose the Au^I monomer ($AuOH/m\text{-}ZrO_2(\bar{2}12)$) as the active species for the hydrogenation of acrolein.

First, H_2 dissociation over $AuOH/m\text{-}ZrO_2(\bar{2}12)$ was investigated. The reaction profile is shown in Fig. 3. The energy barrier for H_2 dissociation is only 0.52 eV, and the reaction is exothermic by 0.91 eV. It can be seen that the Au–O_{latt} bond must break in order to dissociate H_2, which finally leads to two moieties, H–AuOH and H–O_{latt}. Mulliken charge analysis of the dissociated product shows that the two dissociated H species are quite different in nature: the one on the O_{latt} is proton-like with the net charge being +0.30 |e|, whereas the other H on Au^I is negatively charged (−0.05 |e|) and is thus hydride-like. This indicates that H_2 cleavage at AuOH belongs to heterolytic dissociation.

The hydrogenation pathways of acrolein were then explored, in which four different pathways can be distinguished according to the position of acrolein where the first H attaches, as shown in Scheme 1. For clarity, these four different possible pathways are labeled as PATH I, PATH II, PATH III, and PATH IV (Scheme 1). It should be noticed that the reaction network in the single Au system is much simpler than that determined on transition metal surfaces [5,8], which will be discussed later. From our calculations, acrolein only weakly adsorbs near the Au^I with the adsorption energy being 0.21 eV. It is therefore very likely that the initial hydrogenation reaction follows an Eley–Rideal mechanism, where the gas phase acrolein reacts directly with the dissociated H on the surface. In the following, our results for the four different paths are elaborated.

PATH I. The first hydrogenation in this path occurs by the H (proton) on the O_{latt} attaching to the O end of acrolein, as shown in Fig. 4. This step is facile with only 0.31 eV energy barrier. At the located TS (TS1) the distance between H and O_{latt} is 1.36 Å, and that between O (acrolein) and H is 1.12 Å. After the TS1, the newly formed intermediate state (MS) [$CH_2CHCHOH$] adsorbs at the Au center. At this MS (MS1), the hydride of Au can shift to the α-C position (see Scheme 1) to yield allyl alcohol by surmounting a second TS (TS2) with 0.22 eV energy barrier. It is noticed that the MS1 is kinetically unstable: it can also decay easily back to the IS with only 0.07 eV barrier. According to the kinetics theory, we can deduced that the overall energy barrier for the formation of allyl alcohol is no more than 0.46 eV, which is the energy difference between TS2 and the initial state (IS) (see Fig. 4).

It should be emphasized that a linear structure of the Au cation is always preserved during the whole reaction. The reaction starts from the two-coordinated linear AuOH on the oxide support. To

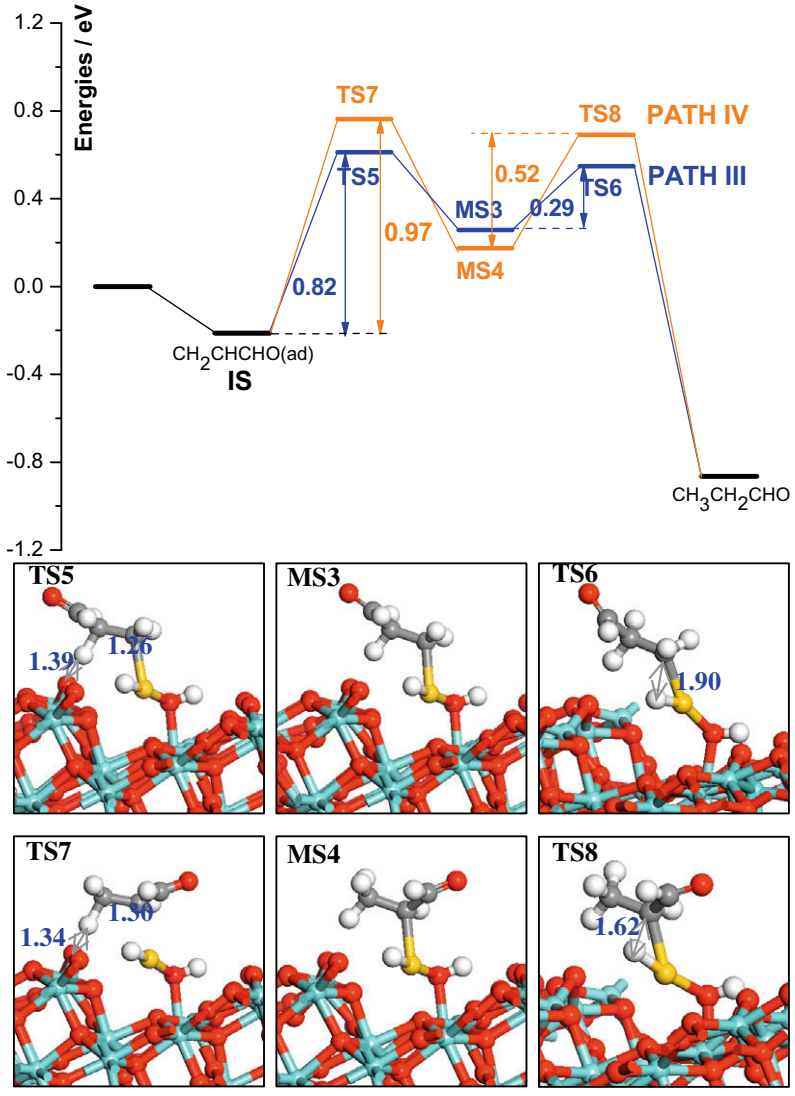

Fig. 5. Reaction profiles of the hydrogenation of acrolein to propanal on $AuOH/m\text{-}ZrO_2(\bar{2}12)$. Also shown are the structures (lateral views) of TS, and the MS.

dissociate H_2, the original Au–O_{latt} bond breaks in order to accommodate two extra H atoms. The subsequent hydrogenation reactions occur similarly to those identified in homogeneous catalysis, where the coming reactant and the leaving product act as the ligand of the Au cation [49]. It can be concluded that the oxides with proper acid-base properties are essential for the hydrogenation reaction, since m-ZrO_2 here not only serves as a base to provide sites for H_2 dissociation, but also subsequently as an acid for the hydrogenation of double bonds [33].

PATH II. Alternative to PATH I, the H on the O_{latt} atom may firstly react with the α-C atom of acrolein. However, we found that this reaction channel is kinetically inhibited due to a very high reaction barrier (2.07 eV). At the TS (TS3), the distance between H and O_{latt} is 1.47 Å, and that between α-C and H is 1.23 Å, as shown in Fig. 4. In consistent with the high barrier, the adsorbed intermediate (MS2) is about 1.90 eV less stable than the IS. Therefore, we can safely rule out PATH II as a possibility to produce allyl alcohol due to the highly unfavorable energetics.

PATHs III and IV. Both paths lead to propanal, in which the C=C of acrolein is hydrogenated. In PATH III, the H on the O_{latt} attaches to the β-C of acrolein first, while the γ-C of acrolein is hydrogenated first in PATH IV. The first hydrogenation barriers of the two paths are similar, 0.82 eV for PATH III and 0.97 eV for PATH IV. As shown in Fig. 5, the second hydrogenation is generally easier with a lower reaction barrier. Despite the fact that the final product propanal is about 0.8 eV more stable than allyl alcohol in thermodynamics, PATHs III and IV are kinetically more difficult than PATH I.

The above-mentioned results show that the lowest energy barrier to allyl alcohol is 0.46 eV, whereas that to propanal is 0.82 eV. It is thus expected from kinetics that a good selectivity to allyl alcohol is achievable by selectively catalyzing the hydrogenation of the C=O while avoiding the hydrogenation of the C=C bond. Naturally, one would wonder why the barrier of PATH I is so low. We may understand this as follows. The dissociated H atoms are strongly polarized, being proton-like and hydride-like. As a result, the first hydrogenation step is facilitated by the strong electrostatic interaction between the negative O end of acrolein and the proton on the O_{latt}. Once the O of acrolein is protonated, the next hydrogenation is again facile between the positively charged α-C and the hydride.

Finally, we also examined the reaction channel for the hydrogenation of allyl alcohol to propyl alcohol on AuOH/m-ZrO_2($\bar{2}$12). The deep hydrogenation may occur as a secondary process if the newly produced allyl alcohol reacts further with the dissociated H on another AuOH/m-ZrO_2($\bar{2}$12). Our calculated reaction profile is shown in Fig. 6. We found that the energy barriers are always larger than 0.70 eV no matter which C atoms (β-C or γ-C) are involved to react with the proton on the O_{latt} in the first hydrogenation step.

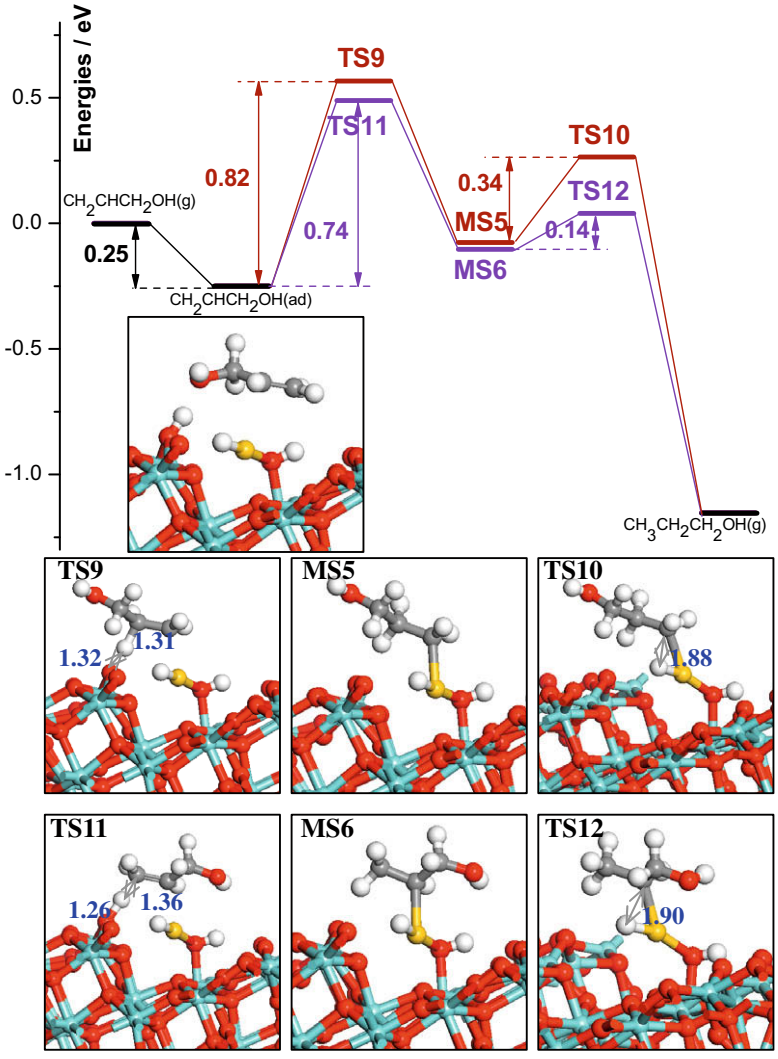

Fig. 6. Reaction profiles of the hydrogenation of allyl alcohol to propyl alcohol on AuOH/m-ZrO_2($\bar{2}$12). Also shown are the structures (lateral views) of the IS, TS, and the MS.

Overall, our results show that it is possible to tune the catalytic temperature to only allow for the hydrogenation of C=O bond in acrolein (0.46 eV barrier), while prohibit all the other side reactions at the mean time (according to the rate equation, 0.24 eV difference in barrier means 10^5 difference in reaction rate at the room temperature if all the other kinetic parameters are the same). It should also be mentioned that the low reaction barrier in hydrogenation is in line with the stability of Au monomers at the oxide steps: the hydrogenation can occur below the room temperature when the specific Au monomer structures are stable enough. Considering that Au clusters are always present on the terraces of oxides, the real picture for the catalytic hydrogenation may in fact be a mixed story. Both Au monomer species at oxide defects (minority species) and Au clusters on oxide terraces (majority species) can contribute to the activity and the selectivity.

It is of interest to further compare our data with the results previously computed for acrolein hydrogenation on Pt(1 1 1). On metal surfaces, the reaction channels are more complex and it is essential to consider surface intermediates produced from 1,3-, 1,4-, or 2,4-hydrogenation steps [5,8]. In these cases, Langmuir–Hinshelwood mechanism is followed in all hydrogenation steps and the produced 'radical' intermediates adsorb strongly on metal surfaces. By contrast, for the single-Au heterogeneous catalysts, there is only one adsorption site with single metal ion (i.e. Au^I) and no other free sites are available to accommodate possible radical-like intermediates. Such radicals include the π-allylic or oxo-π-allylic species after the first hydrogenation step, which are found to be very unstable in the single Au system. Taking PATH I as the example, we showed that once the O is hydrogenated, only the α-C can adsorb on Au^I and finally pick up the hydride. This is because the α-C is geometrically closest to Au^I (e.g. γ-C is too far away from Au^I), and it evolves bonding with Au at the TS naturally (Fig. 4). Consequently, the reaction network is largely simplified, which is an important feature of the single Au catalysis.

Energetically, Loffreda et al. showed that the reaction barrier for the hydrogenation of the C=O bond is smaller than that for the hydrogenation of the C=C bond [5,8], and the magnitude of preference (0.5 eV) is similar to that in our Au^I/ZrO_2 system. However, due to the larger adsorption energy of allyl alcohol than that of propanal on Pt(1 1 1), the major product will be the saturated aldehyde. They concluded that the desorption step controls largely the selectivity of the acrolein hydrogenation on Pt. By contrast, both acrolein and the products including allyl alcohol adsorb weakly on AuOH/m-ZrO_2. Consequently, the desorption of the partial hydrogenation product is not a problem any more. The good selectivity is however at the expense of the activity. From our results, it can be found that the initial hydrogenation follows the Eley–Rideal mechanism due to the low adsorption energy of acrolein and thus the reaction should be intrinsically slow with a low preexponential factor in rate equation. Our results here are consistent with the general finding in heterogeneous catalysis: the activity and the selectivity are often reversely correlated. Although the single Au catalyst can exhibit a high selectivity to the partial hydrogenation product, its overall activity of hydrogenation may be not satisfactory compared to traditional metal catalysts.

4. Conclusion

This work represents our attempt to predict the catalytic performance of oxide-supported single gold catalysts for the selective hydrogenation of acrolein from theory. Both the thermodynamics on the stability of the catalyst and the kinetics for the hydrogenation pathways were explored within the framework of DFT periodic calculations.

From thermodynamics, we showed that the flat m-ZrO_2 surface only supports metallic Au clusters due to its low adsorption energy toward Au monomers. On the other hand, Au^{III} cations can be stable at the stepped m-ZrO_2 surface (represented by m-$ZrO_2(\bar{2}\,1\,2)$) up to 350 K at oxidizing conditions. Next, the hydrogenation mechanism of acrolein on AuOH/m-$ZrO_2(\bar{2}\,1\,2)$ was examined since Au^{III} can be readily reduced to Au^I under H_2 pressure from the thermodynamics at the reducing environment and our previous work [33]. We found that H_2 can dissociate on Au^I(AuOH) heterolytically with a barrier of 0.52 eV. More importantly, AuOH/m-$ZrO_2(\bar{2}\,1\,2)$ does exhibit a high selectivity for the hydrogenation of acrolein to allyl alcohol. The reaction barrier to the desired molecule is only 0.46 eV, whilst the barriers to other byproducts are at least 0.24 eV higher. The deep hydrogenation to propyl alcohol can also be prevented kinetically. The picture presented here would benefit the rational catalyst design by tuning the metal/oxide properties, and maybe more importantly, provide the hope for theory to predict the selectivity of complex catalytic process over multicomponent materials.

Acknowledgments

This work is supported by NSF of China (20825311, 20773026, 20721063, J0730419, 20673024), Science & Technology Commission of Shanghai Municipality (08DZ2270500) and the Program for Professor of Special Appointment (Eastern Scholar) at Shanghai Institutions of Higher Learning.

References

[1] P. Gallezot, D. Richard, Catal. Rev.-Sci. Eng. 40 (1998) 81.
[2] T. Marinelli, V. Ponec, J. Catal. 156 (1995) 51.
[3] P. Claus, Top. Catal. 5 (1998) 51.
[4] F. Delbecq, P. Sautet, J. Catal. 152 (1995) 217.
[5] D. Loffreda, F. Delbecq, F. Vigne, P. Sautet, Angew. Chem. Int. Ed. 44 (2005) 5279.
[6] D. Loffreda, F. Delbecq, P. Sautet, Chem. Phys. Lett. 405 (2005) 434.
[7] D. Loffreda, Surf. Sci. 600 (2006) 2103.
[8] D. Loffreda, F. Delbecq, F. Vigne, P. Sautet, J. Am. Chem. Soc. 128 (2006) 1316.
[9] F. Delbecq, P. Sautet, J. Catal. 211 (2002) 398.
[10] D. Loffreda, Y. Jugnet, F. Delbecq, J.C. Bertolini, P. Sautet, J. Phys. Chem. B 108 (2004) 9085.
[11] P. Claus, A. Bruckner, C. Mohr, H. Hofmeister, J. Am. Chem. Soc. 122 (2000) 11430.
[12] F. Delbecq, P. Sautet, J. Catal. 220 (2003) 115.
[13] R. Hirschl, F. Delbecq, P. Sautet, J. Hafner, J. Catal. 217 (2003) 354.
[14] W. Grunert, A. Bruckner, H. Hofmeister, P. Claus, J. Phys. Chem. B 108 (2004) 5709.
[15] M. Bron, D. Teschner, A. Knop-Gericke, A. Scheybal, B. Steinhauer, M. Havecker, R. Fodisch, D. Honicke, R. Schlogl, P. Claus, Catal. Commun. 6 (2005) 371.
[16] A.S.K. Hashmi, G.J. Hutchings, Angew. Chem. Int. Ed. 45 (2006) 7896.
[17] G.C. Bond, D.T. Thompson, Catal. Rev.-Sci. Eng. 41 (1999) 319.
[18] C. Milone, M.L. Tropeano, G. Gulino, G. Neri, R. Ingoglia, S. Galvagno, Chem. Commun. (2002) 868.
[19] J.E. Bailie, H.A. Abdullah, J.A. Anderson, C.H. Rochester, N.V. Richardson, N. Hodge, J.G. Zhang, A. Burrows, C.J. Kiely, G.J. Hutchings, Phys. Chem. Chem. Phys. 3 (2001) 4113.
[20] P. Claus, H. Hofmeister, C. Mohr, Gold Bull. 37 (2004) 181.
[21] J.E. Bailie, G.J. Hutchings, Chem. Commun. (1999) 2151.
[22] C. Mohr, H. Hofmeister, J. Radnik, P. Claus, J. Am. Chem. Soc. 125 (2003) 1905.
[23] S. Schimpf, M. Lucas, C. Mohr, U. Rodemerck, A. Bruckner, J. Radnik, H. Hofmeister, P. Claus, Catal. Today 72 (2002) 63.
[24] C. Mohr, H. Hofmeister, P. Claus, J. Catal. 213 (2003) 86.
[25] R. Radnik, C. Mohr, P. Claus, Phys. Chem. Chem. Phys. 5 (2003) 172.
[26] C. Mohr, N. Hofmeister, M. Lucas, P. Claus, Chem. Eng. Tech. 23 (2000) 324.
[27] J.M. Thomas, R. Raja, D.W. Lewis, Angew. Chem. Int. Ed. 44 (2005) 6456.
[28] J.C. Fierro-Gonzalez, B.C. Gates, Chem. Soc. Rev. 37 (2008) 2127.
[29] J. Guzman, B.C. Gates, Angew. Chem. Int. Ed. 42 (2003) 690.
[30] J.C. Fierro-Gonzalez, B.C. Gates, J. Phys. Chem. B 108 (2004) 16999.
[31] X. Zhang, H. Shi, B.Q. Xu, Angew. Chem. Int. Ed. 44 (2005) 7132.
[32] X. Zhang, A. Corma, Angew. Chem. Int. Ed. 47 (2008) 4358.
[33] Z.P. Liu, C.M. Wang, K.N. Fan, Angew. Chem. Int. Ed. 45 (2006) 6865.
[34] J.M. Soler, E. Artacho, J.D. Gale, A. Garcia, J. Junquera, P. Ordejon, D. Sanchez-Portal, J. Phys.-Condens. Matter 14 (2002) 2745.
[35] J. Junquera, O. Paz, D. Sanchez-Portal, E. Artacho, Phys. Rev. B 64 (2001) 235111.
[36] N. Troullier, J.L. Martins, Phys. Rev. B 43 (1991) 1993.

[37] J.P. Perdew, K. Burke, M. Ernzerhof, Phys. Rev. Lett. 77 (1996) 3865.
[38] Z.P. Liu, P. Hu, A. Alavi, J. Am. Chem. Soc. 124 (2002) 14770.
[39] Z.P. Liu, P. Hu, J. Am. Chem. Soc. 125 (2003) 1958.
[40] Z.P. Liu, X.Q. Gong, J. Kohanoff, C. Sanchez, P. Hu, Phys. Rev. Lett. 91 (2003) 266102.
[41] H.F. Wang, Z.P. Liu, J. Am. Chem. Soc. 130 (2008) 10996.
[42] A. Christensen, E.A. Carter, Phys. Rev. B 58 (1998) 8050.
[43] C.M. Wang, K.N. Fan, Z.P. Liu, J. Am. Chem. Soc. 129 (2007) 2642.
[44] Q.L. Tang, Q.J. Hong, Z.P. Liu, J. Catal. 263 (2009) 114.
[45] K. Reuter, M. Scheffler, Phys. Rev. B 65 (2002) 035406.
[46] G.S. Shafai, S. Shetty, S. Krishnamurty, V. Shah, D.G. Kanhere, J. Chem. Phys. 126 (2007) 014704.
[47] A. Hoffmann-Roder, N. Krause, Org. Biomol. Chem. 3 (2005) 387.
[48] P. Pyykko, Angew. Chem. Int. Ed. 43 (2004) 4412.
[49] A. Comas-Vives, C. Gonzalez-Arellano, A. Corma, M. Iglesias, F. Sanchez, G. Ujaque, J. Am. Chem. Soc. 128 (2006) 4756.